Research Article | Vol. 29, No. 24 / 22 Nov 2021 / Optics Express 39696
Optics EXPRESS

Dual color DMD-SIM by temperature-controlled laser wavelength matching

MARIO LACHETTA,[1,2,3] GERD WIEBUSCH,[1] WOLFGANG HÜBNER,[1,3] JAN SCHULTE AM ESCH,[2,3] THOMAS HUSER,[1,3,4] AND MARCEL MÜLLER[1,5]

[1]*Biomolecular Photonics, Faculty of Physics, Bielefeld University, Universitätsstraße 25, 33615 Bielefeld, Germany*
[2]*Department of General and Visceral Surgery, Protestant Hospital of Bethel Foundation, Schildescher Str. 99, 33611 Bielefeld, Germany*
[3]*Forschungsverbund BioMedizin Bielefeld, FBMB, Maraweg 21, 33617 Bielefeld, Germany*
[4]*thomas.huser@physik.uni-bielefeld.de*
[5]*muellerphysics@gmail.com*

Abstract: Structured illumination microscopy (SIM) is a fast and gentle super-resolution fluorescence imaging technique, featuring live-cell compatible excitation light levels and high imaging speeds. To achieve SIM, spatial modulation of the fluorescence excitation light is employed. This is typically achieved by interfering coherent laser beams in the sample plane, which are often created by spatial light modulators (SLMs). Digital micromirror devices (DMDs) are a form of SLMs with certain advantages, such as high speed, low cost and wide availability, which present certain hurdles in their implementation, mainly the blazed grating effect caused by the jagged surface structure of the tilted mirrors. Recent works have studied this effect through modelling, simulations and experiments, and laid out possible implementations of multi-color SIM imaging based on DMDs. Here, we present an implementation of a dual-color DMD based SIM microscope using temperature-controlled wavelength matching. By carefully controlling the output wavelength of a diode laser by temperature, we can tune two laser wavelengths in such a way that no opto-mechanical realignment of the SIM setup is necessary when switching between both wavelengths. This reduces system complexity and increases imaging speed. With measurements on nano-bead reference samples, as well as the actin skeleton and membrane of fixed U2OS cells, we demonstrate the capabilities of the setup.

1. Introduction

Structured illumination microscopy illuminates a fluorescent sample with a sinusoidal intensity pattern of high spatial frequency and ideally high contrast, to extract previously unobservable information from the sample [1,2]. Nowadays, SIM is utilized in a large variety of applications in cell biology, especially when high imaging speeds [3–8] or live-cell compatible imaging [3,5,9–11] is needed.

State-of-the-art tools for the generation of these SIM interference patterns are spatial light modulators (SLMs). These can be divided into two main groups, where one group consists of liquid crystal based systems, where devices with binary pixels reach very high speeds [3–7], and the other group consists of digital micromirror devices, which also feature high speed and low cost [8,12] and are available in a variety of form factors.

A critical problem when employing DMDs in combination with coherent light sources (as required in interference pattern-based SIM) is the blazed grating effect. The blazed grating effect arises due to the device's jagged pixel structure and results in different, angle-dependent reflectivities for the diffraction orders that form the interference pattern. This results in poor pattern contrast for specific illumination angles. Using both experimental setups and in-depth

#437822 https://doi.org/10.1364/OE.437822
Journal © 2021 Received 2 Aug 2021; revised 17 Sep 2021; accepted 11 Oct 2021; published 15 Nov 2021

Optics EXPRESS

simulation, we were recently able to model this blazed grating effect and to successfully employ DMDs as light modulators for SIM [8,13].

The blazed grating effect also leads to specific alignment requirements if multiple different excitation wavelengths are required to conduct an imaging experiment [12,13]. In short, either the angle of incidence towards the DMD has to be readjusted when switching between excitation wavelengths or the wavelength combinations need to be matched in such a way that they can share the same angle of incidence. The first solution, using a separate angle of incidence for each of three different excitation wavelengths, was recently demonstrated by Brown et. al. [12]. In their implementation, two of the wavelengths almost exhibited the correct ratio required for matching their optimal angle of incidence, thus, a voice-coil controlled mirror was employed to slightly adjust the beam path when switching between the two wavelengths, while a third wavelength used a separate optical path. Although this is an elegant solution to the blazed grating problem, this approach comes with some opto-mechanical complexity which we wanted to avoid.

Another solution to the problem at hand is to maintain a fixed angle of incidence, and instead match the two excitation wavelengths in such a way that the wavelength pair can share the same optical path. Possible wavelength combinations have been identified in simulations [13] and are linked to an integer ratio (3:4) of the corresponding wavelengths. Potential combinations such as 488.00 nm & 650.67 nm, or 473.00 nm & 630.67 nm can share a common angle of incidence towards the DMD.

Wavelengths of 473 nm and 488 nm are readily available in many laboratories based on diode-pumped solid-state lasers (DPSS). As DPSS systems, their output wavelength is very stable, whereas lasers in the red wavelength range (635 nm to 660 nm) are widely available as diode lasers. The output wavelength of diode lasers is less stable and easily shifts by the temperature of the diode. While this is usually an undesirable effect that needs to be controlled, in our application we can exploit this effect to finely tune the diode's output wavelength to achieve the proper combination required for a two-color DMD SIM setup.

2. Results

The previously mentioned blazed-grating effect essentially describes the superposition of the diffraction image of a grating with the diffraction image of a single grating point (envelope). In the case of DMDs, this is the superposition of the diffraction image of the native DMD grating with the diffraction image of a single mirror. The diffraction orders of the patterns displayed on the DMD form around the diffraction orders of the native grating (see Supplement 1, Fig. S1). A one-dimensional description of the blazed-grating effect [14] is not sufficient to fully reflect the two-dimensional nature of DMDs. However, a few publications have previously investigated the blazed-grating effect of DMDs with coherent light, especially for SIM microscopy [8,13,15].

We use the following coordinates to describe the angles of incidence $\vec{a} = (a_x, a_y, a_z)$ and emergence $\vec{b} = (b_x, b_y, b_z)$ to and from the DMD (see Fig. 1) [8,13]:

$$\vec{a}\,(\varphi_a, \vartheta_a) = \begin{pmatrix} a_z \cdot \tan(\varphi_a) \\ a_z \cdot \tan(\vartheta_a) \\ a_z \end{pmatrix} \quad \text{with} \quad a_z = \sqrt{\frac{1}{\tan^2(\varphi_a)+\tan^2(\vartheta_a)+1}} \tag{1}$$

$$\vec{b}(\varphi_b, \vartheta_b) = \begin{pmatrix} b_z \cdot \tan(\varphi_b) \\ b_z \cdot \tan(\vartheta_b) \\ b_z \end{pmatrix} \quad \text{with} \quad b_z = \sqrt{\frac{1}{\tan^2(\varphi_b) + \tan^2(\vartheta_b) + 1}}$$

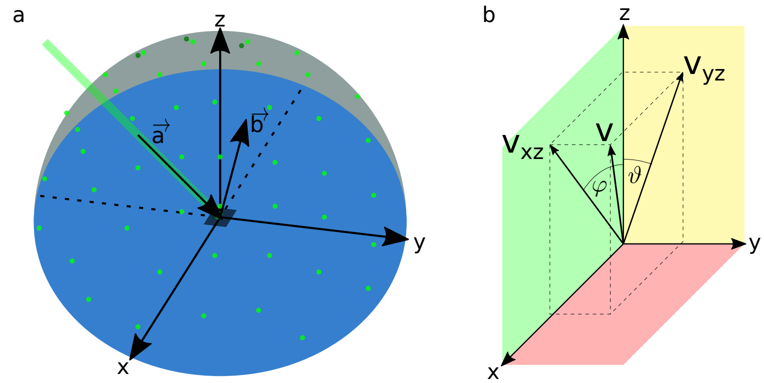

Fig. 1. Visualization of the incident and emergent angles and the corresponding angle definitions. (a) Schematic representation of a laser beam coming from direction $\vec{a}$ which is reflected/diffracted at the DMD in the origin. The vector $\vec{b}$ represents a specific angle of emergence as an example. The green dots illustrate the resulting diffraction orders of the DMD. (b) Geometric definition of the angular coordinates for $\vec{a}$ and $\vec{b}$. The x and y axes are associated with φ and ϑ, respectively. This figure serves as an introduction to the topic and is therefore taken from our corresponding previous publication [8].

For the angles of incidence α and emergence β along the diagonals perpendicular to the tilting axis of the micromirrors, $\vec{a} = (a_x, -a_x, a_z)$ and $-\varphi_a = \vartheta_a$ are fulfilled [8,13]. It follows that:

$$\alpha = \arctan\left(\sqrt{2} \cdot \tan(\varphi_a)\right) \quad \text{and} \quad \beta = \arctan\left(\sqrt{2} \cdot \tan(\varphi_b)\right) \tag{2}$$

If the angle of incidence is varied, the diffraction orders and the envelope do not move congruently to each other. The direction in which the diffraction orders are found are given by the overall grating structure of the DMD and would occur in the same fashion on any non-jagged, reflective grating with the same dimensions. The direction in which the maximum of the envelope is found, on the other hand, is given by the tilt angle of the mirrors, and would equally occur when using a flat mirror placed at the same angle. To achieve equal intensity distributions in the diffraction orders, the maximum of the envelope has to coincide with a diffraction maximum of the grating. If the center of the envelope does not overlap with the position of a diffraction order of the native grating, the intensity distribution of the diffraction pattern obtained by the DMD becomes asymmetrical. To use a DMD as SLM in a SIM microscope, it is therefore necessary to superimpose the center of the envelope with the position of a diffraction order of the native diffraction grating (blazed condition). This becomes a problem especially when using several different excitation wavelengths (see Fig. 2(a)) since the diffraction orders for different wavelengths arise at different positions.

There are two main solutions to this problem: either vary the angles of incidence for different wavelengths during the operation of the microscope using opto-mechanics (e.g. voice coil mirrors) so that the blazed condition is fulfilled [12] or to choose the wavelengths of the excitation lasers such that at the same angle of incidence, the blazed condition is fulfilled for both wavelengths (see Fig. 2(b)) [13]. The main advantage of the wavelength matching approach is that no moving parts are required in the excitation beam path of the microscope. This significantly improves the stability of the microscope and thus the reproducibility of measurements. For this reason, we consider the wavelength matching approach to be preferable to angle matching. However, the corresponding experimental demonstration of this approach was still open. Here,

Optics EXPRESS

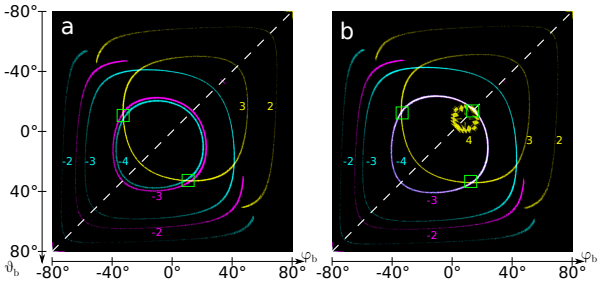

Fig. 2. Blazed condition analysis for multi color diffraction angles. The diffraction space ($-80° \leq \varphi_b,\ \vartheta_b<80°$) was examined for different wavelengths for the blazed condition with the help of simulations. In this case, the blazed condition is fulfilled if the emergence angles of the brightest diffraction order and the envelope differ by less than 0.1°. Angles of incidence were considered between −60° to 60° ($-60° \leq \varphi_a,\ \vartheta_a<60°$). The white dashed line indicates the diagonal perpendicular to the tilting axis of the DMD's micromirrors. The colored numbers serve to identify the numeration of the diffraction orders. $\gamma^{\pm} = \pm 12°$ was chosen as the tilt angle of the micromirrors. (a) Wavelengths typical for excitation in fluorescent imaging are shown, with 488 nm (cyan) & 638 nm (magenta) for γ^- and 561 nm (yellow) for γ^+ [13]. The green boxes mark possible two-color configurations (488 nm with 561 nm and 638 nm with 561 nm) off the diagonal. (b) Wavelengths optimized for three-color combinations 473 nm (cyan) & 630.7 nm (magenta) for γ^- and 550.7 nm (yellow) for γ^+ are shown. The three green boxes mark the possible three-colour configurations, one of which is on the diagonal. The strange shape of the blazed condition of the 4th diffraction order at 550.7 nm is due to the blazed condition just evolving (falling wavelength) or collapsing (rising wavelength). This figure serves as an illustration of the wavelengths matching approach and is reproduced from the corresponding previous publication [13].

we demonstrate an implementation of this approach to dual color DMD-SIM microscopy by temperature-controlled wavelength matching.

If two excitation wavelengths λ_1 and λ_2 are in an integer ratio n_2/n_1, a matching condition is fulfilled. The n_1-th and n_2-th diffraction orders then lie on top of each other. Using a DMD with 7.56 µm pixel pitch and a micromirror tilt angle of 12° (e.g. *DLP LightCrafter 6500 (Texas Instruments)* [16]), and by further limiting excitation wavelengths to the visible spectral region and real emergence angles ($-90°<\varphi_b, \vartheta_b<90°$), only the following matching condition remains:

$$\frac{\lambda_1}{\lambda_2} = \frac{n_2}{n_1} = \frac{3}{4} \tag{3}$$

If this matching condition is fulfilled, the 4th and 3rd diffraction order of λ_1 and λ_2 lie on top of each other [13]. If the envelope is now placed at the position of these diffraction orders by adjusting the angle of incidence on the DMD, then the blazed condition is fulfilled for both wavelengths. From Eq. (3), a combination of a blue and a red excitation laser (see Table 1) can be chosen, especially since these wavelengths are also well suited for the excitation of common fluorophores. Table 1 also lists a choice of potential wavelength combinations with lasers that are commercially available.

If the blue and red wavelengths are combined in all possible combinations (Fig. 3(a)), it is noticeable that no combination of currently available laser systems exactly fulfills the matching condition. However, four combinations are very close to the matching condition (see the right-hand column in Table 1). In order for the 4th and 3rd diffraction orders to lie exactly on top of each other, it is necessary to shift one of the excitation wavelength by a few nanometers so that the matching condition is fulfilled. Laser diodes can be shifted by a few nanometers by

Optics EXPRESS

Table 1. Available and chosen laser wavelength combinations.[a]

Blue wavelength	Red wavelength
425 nm	594 nm
445 nm	633 nm
450 nm	637 nm
457 nm	638 nm
458 nm	639,7 nm
460 nm	640 nm
473 nm	642 nm
488 nm	647 nm
491 nm	660 nm
505 nm	

Chosen blue wavelength	Chosen red wavelength	$\frac{\lambda_1}{\lambda_2}$
445 nm	594 nm	0.749
473 nm	633 nm	0.747
488 nm	647 nm	0.754
491 nm	660 nm	0.744

[a]Left: Selection of laser wavelengths available from different manufacturers [17–21]. With regard to wavelength matching, the blue and red wavelength range was defined as 425 nm to 505 nm and 594 nm to 660 nm. Right: Laser wavelength combinations and their ratios that fulfill the matching condition most closely.

changing the diode or case temperature. For such a diode laser to be used as an excitation laser in a SIM microscope, it is necessary that the laser is a single-mode diode laser with at least 50 mW output power. The HL63163DG 633 nm/100 mW laser diode meets these requirements and can be tuned from 629 nm to 636 nm via the case temperature (see Fig. 3(b)) [22]. If the wavelength of the laser diode were set to 630.67 nm, it would be perfectly suited for combination with a 473 nm laser. In Fig. 3(c), we determined how the measured positions of the diffraction orders shift when the laser diode is temperature-tuned. The measured position change of the diffraction orders agrees quite well with the simulated position changes (Fig. 3(d)). The measured wavelength of our blue laser (Spectra Physics Excelsior 473, 473 nm/50 mW) is $\lambda_1 = 473.1\ nm$. At a case temperature of 19°C, the lasing wavelength for red is $\lambda_2 = 630.8\ nm$. This means that the matching condition is now fulfilled for this combination:

$$\frac{\lambda_1}{\lambda_2} = \frac{473.1\ nm}{630.8\ nm} = \frac{3}{4} = 0.75 \tag{4}$$

Employing wavelength shifting through temperature control introduces two more effects relevant for SIM. First, at certain temperatures, the laser undergoes mode jumps, and two adjacent modes lase together (see Supplement 1, Fig. S5). This should be avoided, as it leads to a doubling in the diffraction structures. Additionally, employing a Fourier filter mask in the SIM means that unmatched wavelength (e.g. when not controlling the laser temperature) cannot enter the illumination arm beyond the Fourier filter (see Supplement 1, Fig. S6). Thus, the system cannot be operated without stabilizing the temperature and thus laser wavelength. On the other side, this effect could be used as a feedback mechanism to find and tune the case temperature.

By utilizing these lasers we were able to convert our two-beam DMD-SIM microscope from one excitation color channel (532 nm) to two excitation color channels (473 nm and 631 nm) (see Fig. 4). The DMD is rotated by 45° so that the tilting axis of the micromirrors is perpendicular to the plane of the excitation lasers. The control and live reconstruction software are based on fairSIM-VIGOR [7]. Nine raw images (3 angles with 3 phases each) are recorded per channel and can be reconstructed in real time and stored for later reconstruction and post-processing. At the heart of the timing and synchronization of the camera with the DMD is an Arduino Uno microcontroller. Switching the lasers on and off quickly between SIM raw images is not necessary, as the DMD steers the intensity out of the excitation beam path as soon as a SIM pattern is no longer displayed. To avoid crosstalk between channels, the second excitation laser is shuttered during imaging in one channel, respectively.

Our dual color DMD-SIM microscope, like its single color predecessor [8], can acquire up to 540 raw frames per second. This corresponds to 60 SIM-reconstructed fps in one channel or 30

Optics EXPRESS

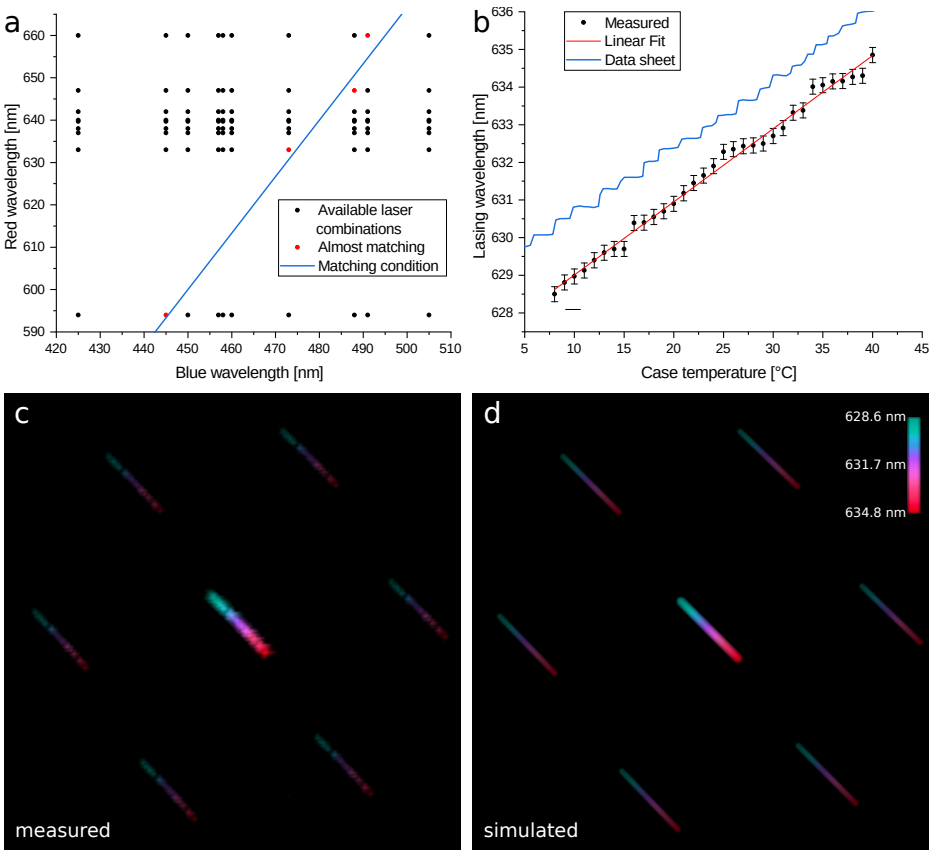

Fig. 3. Matching wavelength and shifting diffraction orders by tuning diode lasing wavelength via temperature. (a) Graphical representation of all possible combinations of commercially available blue and red laser wavelengths (black dots). The blue line shows the required matching condition, where the blue wavelength is ¾ of the red wavelength. The lasers represented by red dots almost fulfill the matching condition. (b) Lasing wavelength of the laser diode (HL63163DG) from data sheet (blue) and measured (black) with RGB-Photonics Qwave Compact Spectrometer as a function of the case temperature measured by the control unit. During the measurement, the laboratory temperature was 20°C and the diode current was kept at a constant 170 mA. The red line corresponds to the linear fit through all measured data points. The deviation between the measured data points and the data sheet can be explained by the usual manufacturing tolerance of 633 nm ± 3 nm for the lasing wavelength of the laser diode. Both the measured data and the data from the data sheet show mode jumps, as is usual for a laser diode (details in the method section of the supplemental document). (c) Color-coded measured diffraction images (1.3° × 1.3° / 4.5 mm x 4.5 mm) of the DMD as a function of the lasing wavelength (628.6 nm to 634.8 nm) of the laser diode in logarithmic intensity representation. Measured with an IDS uEye UI-3060CP-M-GL Rev.2 CMOS camera in the Fourier plane of the setup (Fig. 4). The small irregularities are caused by mode hops in the laser diode. (d) Color-coded simulated diffraction images (1.3° × 1.3°) of the DMD as a function of the lasing wavelength (628.6 nm to 634.8 nm) of the laser diode in logarithmic intensity representation. The simulation was conducted with 350×350 individual mirrors, with a grating constant of m=7.56 µm, a tilt angle of $\gamma = 12°$ and an incidence angle of $\alpha = 43.7°$ ($\varphi_a = -\vartheta_a = 34.05°$). The SIM patterns used are those of the 631 nm channel. All diffraction images shown are integrated over the three SIM angles.

Optics EXPRESS

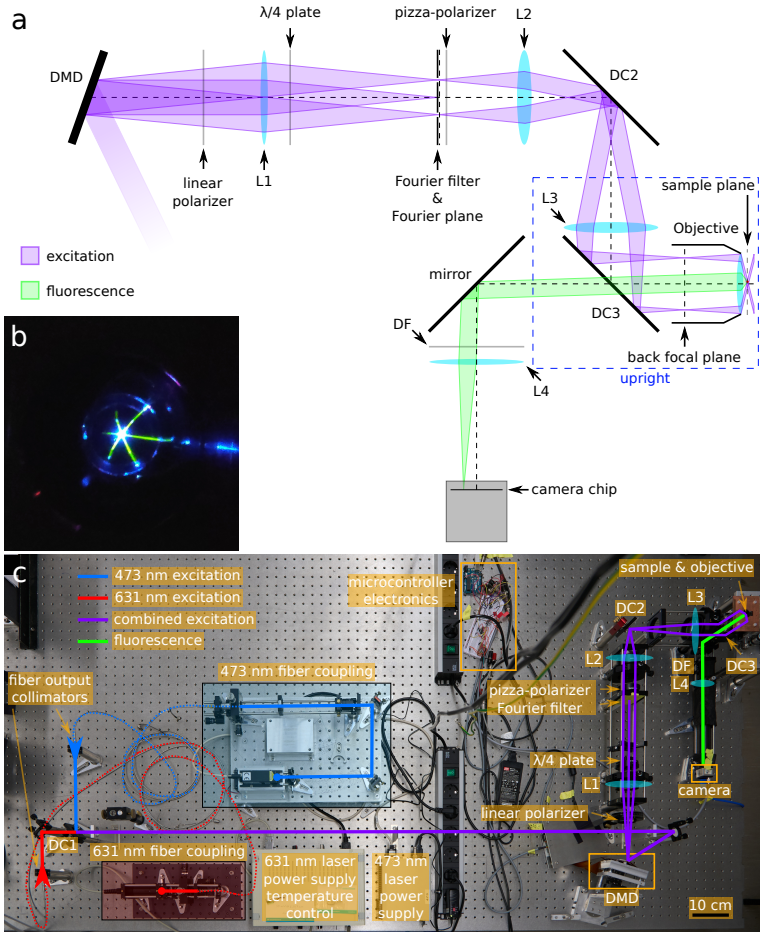

Fig. 4. The dual color DMD SIM Microscope. (a) Schematic representation of the setup. (b) Photo taken from above the objective lens with 473 nm excitation while two beams for each of the three SIM angles propagate through each other in the sample (in this case water on a cover glass). (c) Photo of the custom-built two-color DMD-SIM microscope. For excitation, 473 nm (blue) and 631 nm (red) laser beams are coupled into two separate single mode fibers. Behind the fibers, the two s-polarized and collimated beams with diameters of 18.5 mm FWHM are superimposed (purple) by means of dichroic mirror DC1 before they hit the DMD at an angle of approx. $\alpha = 43.7°$. The laser beams reflected/diffracted by the DMD at an angle of approx. $\beta = -19.7°$ create the Fourier plane at the position of the Fourier filter by passing through lens L1. The linear polarizer, the λ/4 plate and the pizza-polarizer ensure the correct linear alignment of the polarization of the individual SIM angles [23]. Lenses L2 and L3 act as a telescope, focusing the laser beams filtered by the Fourier filter into the back focal plane of the objective. The objective collimates the focused laser beams and causes them to propagate through each other in the sample plane, resulting in the desired sinusoidal SIM pattern in the sample due to interference. Two dichroic mirrors DC2 and DC3 are used to compensate the different phase delay off s- and p-polarized light and thus maintain the linear polarization of the excitation light (details in the method section of the Supplement 1). The fluorescence emitted by the sample is collected by the objective. The dichroic mirror DC3 separates the fluorescence light (green) from the excitation light. The detection filter DF additionally blocks excitation light before the fluorescence light is focused on the camera by means of the tube lens L4. The component list is part of the method section of the Supplement 1.

Optics EXPRESS

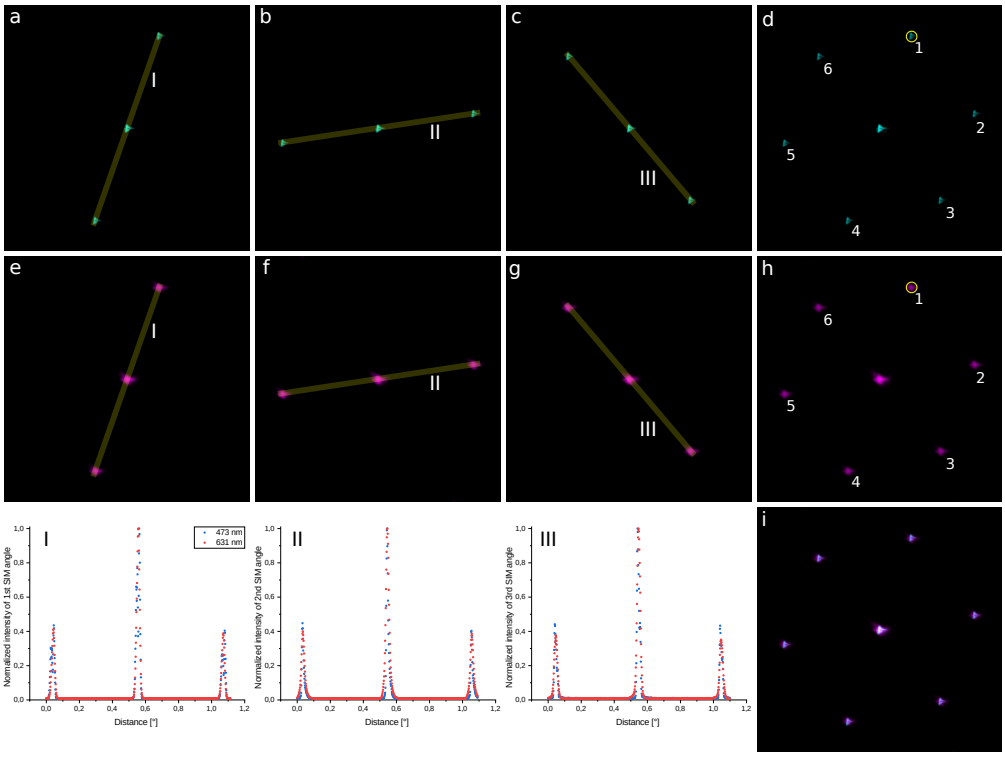

Fig. 5. Fourier plane and diffraction order analysis. Diffraction image (1.3° × 1.3° / 4.5 mm x 4.5 mm) in the Fourier plane of the setup of the individual three SIM angles at 473 nm (a-c) and 631 nm (e-g) in logarithmic intensity representation. All images were acquired with an industrial grade CMOS camera (IDS uEye UI-3060CP-M-GL Rev.2) held in the Fourier plane of the setup. (I-III) Cross-section plots (10 pixels / 0.017° wide) through the diffraction maxima in the Fourier plane at 473 nm (blue) and 631 nm (red). (d, h & i) Summed diffraction images at 473 nm (d), 631 nm (h) and superimposed (i) in logarithmic intensity representation. The small yellow circle in (d & h) indicates the area for the measured spot intensities in Table S1.

in both channels. This surpasses most currently commercially available SIM microscope systems. By using either a faster camera or a combination of two cameras (one for each color channel), the system could be sped up further. When not considering camera read-out speed, the system is only limited by the DMD's switching speed (105 µs) and the exposure time required to successfully acquire a SIM image. The latter is typically limited by the brightness and photostability of the biological sample and the fluorescent dyes used for labelling.

The angle of emergence from the DMD is approx. $\beta = -19.7°$. If the DMD is viewed at an angle, the patterns displayed on it will be distorted. This shear must be taken into account when selecting the SIM patterns to use. The Fiji plugin "fastSIM-GratingSearch" allows to calculate SIM patterns for multi color SIM microscopes [24]. To allow the algorithm to consider the shear of the patterns, we have extended it accordingly. Figure 5 shows that the diffraction orders of both channels lie on top of each other and that the −1st and +1st diffraction order of the SIM pattern are placed symmetrically with the same distance around the central 0th diffraction order. The intensity of the diffraction orders differs by less than 9%. If we look at the deviation of the brightest pixels of the diffraction orders from each other, the difference is a maximum of 15%.

Optics EXPRESS

These deviations are small enough to successfully operate a SIM microscope. As a cross-check, we have also simulated the Fourier plane. The measured and simulated Fourier planes are in good agreement (see Supplement 1, Fig. S2).

We have designed our SIM patterns to achieve a resolution increase of 1.65, which corresponds to a pattern spacing (in sample space) of 274 nm (for 473 nm excitation) and 365 nm (for 631 nm excitation), respectively. Due to the Stokes shift, the fluorescence has a longer wavelength than the excitation. Therefore, the cut-off frequency (Abbe limit) of the detection is smaller than that of the excitation, and effective lateral resolution increase of about 1.7 can be expected from the SIM reconstructions. Even though it is possible to achieve lateral resolution increases of up to a factor of 2.0 with SIM microscopes and even more with TIRF-SIM, it is often not sensible to do so. By choosing a slightly coarser pattern, lateral resolution improvement in 2D SIM is traded for the capability of optical sectioning [25,26] implemented in post-processing as so-called 'OTF attenuation' or 'notch filtering'. When using an SLM, the pattern spacing can also easily be adjusted, and by switching the filter mask, different tradeoffs can be chosen depending on the sample at hand [27].

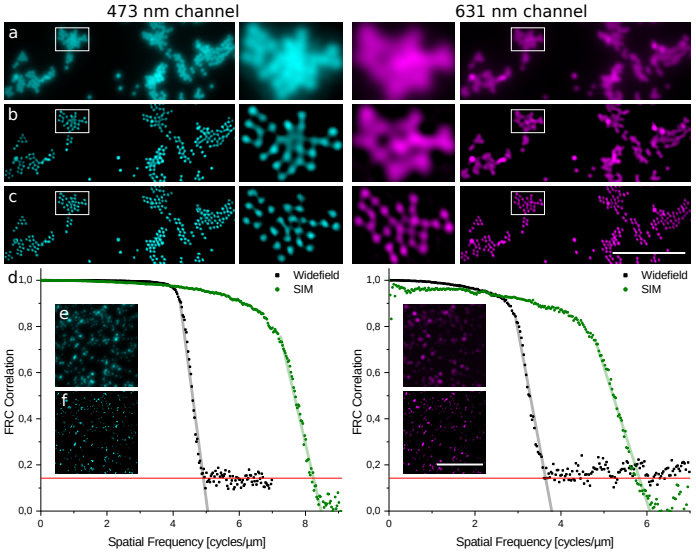

Fig. 6. 200 nm fluorescent beads and FRC statistics on 100 nm fluorescent Beads. The left and right columns correspond to measurements in the 473 nm and 631 nm color channels. (a-b) show images of 200 nm fluorescent beads (scalebar 5 µm, 200 ms / 50 ms exposure time per raw image for the 473 nm / 631 nm channel). (line a) Summed wide-field image of the nine raw SIM images, (line b) Wiener-filtered wide-field image, (line c) SIM reconstruction with fairSIM [30]. In the 2.1 µm x 1.6 µm magnifications, individual beads are distinguishable in the SIM reconstruction, which are not distinguishable in the wide-field or filtered image. (d) FRC analysis [28,29] on 100 nm fluorescent beads from (e) widefield and (f) SIM reconstructions (scalebar 5 µm, 200 ms exposure time per raw image for both channels). The spatial frequency at which the linear fit of the FRC data points falls below a correlation of 1/7 was used to determine the resolution. This results in 203.5 nm ± 8.2 nm (wide field) and 121.3 nm ± 3.4 nm (SIM) for the 473 nm channel and 274.7 nm ± 13.9 nm (wide field) and 171.7 nm ± 4.7 nm (SIM) for the 631 nm channel. This corresponds to a resolution increase of 1.68 ± 0.08 (473 nm channel) and 1.6 ± 0.09 (631 nm channel). The determined and expected resolution increases match.

To prove the function and quality of the microscope, we acquired images of 200 nm and 100 nm fluorescent beads. Comparing the SIM reconstructions of the 200 nm fluorescent beads

Optics EXPRESS

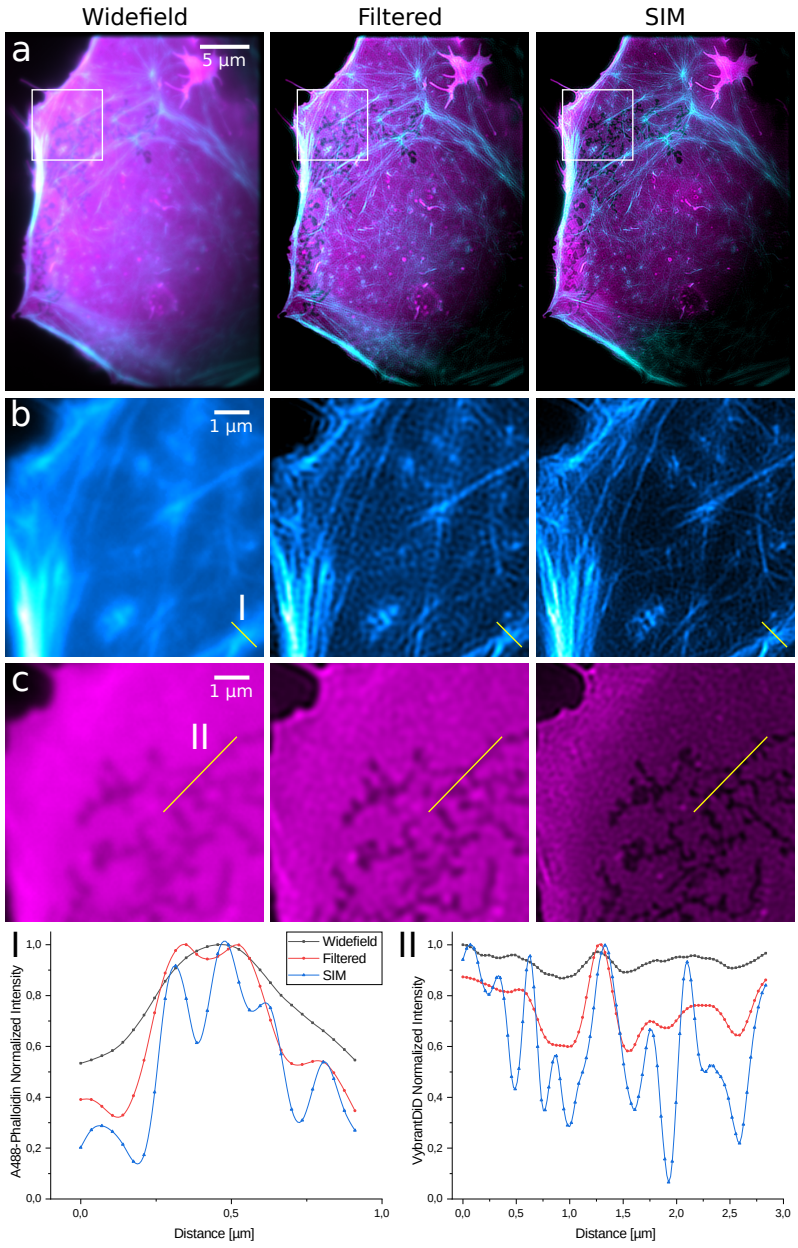

Fig. 7. Dual color fluorescent micrographs of a fixed U2OS cell. Fluorescent micrographs of a fixed U2OS cell (200 ms exposure time) shown as an overlay (row a) of actin (Alexa 488 phalloidin) in the 473 nm channel (row b) and the membrane (Vybrant DiD) in the 631 nm channel (row c). In the fairSIM [30] reconstruction (3rd column), structures are resolved in both channels which are not detectable in the wide-field (1st column) and Wiener filtered image (2nd column). The cross-section plot (I) illustrates that in the SIM reconstruction closely spaced actin filaments can be distinguished from each other, which cannot be separated in the wide-field and Wiener-filtered image. The same can be observed in cross-section plot (II) based on the unstained areas of the plasma membrane. In the SIM reconstruction, many unstained areas in the membrane are visible, which blur into each other in the wide-field and Wiener-filtered image.

Optics EXPRESS

(Fig. 6(c)) with the wide-field (Fig. 6(a)) or Wiener filtered data (Fig. 6(b)), it is easy to see that a noticeable increase in resolution was achieved. To quantify the actual spatial resolution achieved with this setup, we applied the Fourier Ring Correlation (FRC) method to the 100 nm fluorescent beads data (Fig. 6(d)) [28,29]. From the FRC analysis, quantitative numbers for the spatial resolution of 203.5 *nm* ± 8.2 *nm* for the 473 nm channel and 274.7 *nm* ± 13.9 *nm* for the 631 nm channel are obtained for the wide field image (Fig. 6(e)). This is consistent with the Abbe limit lying at 197.4 nm (at 525 nm fluorescence) and 263.6 nm (at 700 nm fluorescence). The resolution of the SIM reconstruction (Fig. 6(f)) determined via FRC analysis is 121.3 *nm* ± 3.4 *nm* (473 nm channel) and 171.7 *nm* ± 4.7 *nm* (631 nm channel). This results in resolution increases of 1.68 ± 0.08 (473 nm channel) and 1.6 ± 0.09 (631 nm channel), which is in good agreement with an expected resolution increase of about 1.7. A further analysis of 100 nm fluorescent beads with cross-section plots are shown in Supplement 1, Fig. S3. Sample preparation is outlined in the Supplement 1.

Figure 7 (and Supplement 1, Fig. S4) displays fluorescence micrographs of the actin skeleton (473 nm channel in cyan) and the membrane (631 nm channel in magenta) of fixed U2OS cells, demonstrating that the microscope is well suited for acquiring images of biological samples. The SIM reconstructions show details that are not visible in the wide-field or Wiener filtered images. The cross-sectional plots of closely spaced actin strands (I) and areas of the membrane (II) that are not stained further illustrate this. It is unclear what caused parts of the membrane to not get stained by the membrane stain. Potential causes could be disruptions in the membrane that occurred e.g. during the process of fixation, or initial staining by fluorophore aggregates, which were washed away later on. The second theory is quite likely based on our observation of brightly stained membrane regions (e.g. in the upper right hand corner or in the lower middle part of the images) which appear to be fluorophore aggregates. Sample preparation is outlined in the Supplement 1.

3. Discussion and conclusion

Our work demonstrates an elegant solution to the problem of using DMDs in multicolor SIM microscopes with coherent excitation light. To deal with the blazed-grating effect, both angle matching and wavelength matching are available. While angle matching was experimentally demonstrated by Peter Brown et. al. [12] and requires additional synchronization measures and optoelectronics, we have successfully demonstrated wavelength matching based on a temperature-tuned diode laser. In our opinion, because of the simpler and thus more stable opto-mechanics, wavelength matching is preferrable to angle matching and easier to implement.

Based on simulations [13], we were able to readily extend a single-color DMD-SIM microscope into a dual-color DMD-SIM microscope. The combination of a blue (DPSS) and red (diode) laser is particularly suitable for wavelength matching. By tuning the diode laser by temperature, the two wavelengths can be brought to the desired ratio of 3/4. With an appropriately selected angle of incidence on the DMD, the position of the envelope coincides with the 4th (blue) and 3rd (red) diffraction order in the diffraction pattern of the DMD. The resulting Fourier plane in the excitation path of a SIM microscope shows a symmetrical intensity distribution of the diffraction orders of the SIM patterns. The measured and simulated effects on the Fourier plane by tuning the red diode laser agree very well.

Since the DMD was not installed perpendicular to the excitation arm, but at an angle of approx. $\beta = -19.7°$, we have extended our grating search algorithm so that it now takes into account the shearing of the spatial frequencies that occurs at this angle. Of course, this feature is not limited to the use of DMDs, but also to FLCoS SLMs if required.

The quality of the high-resolution SIM image reconstructions is comparable to that of systems based on gratings and FLCoS SLMs. The single-color predecessor system was already a

Optics EXPRESS

cost-efficient and very fast SIM microscope [8]. These characteristics have been retained in the conversion to two excitation colors, as they are mainly due to the comparatively low cost of the excitation lasers, the DMD and the camera. The acquisition speed of up to 540 raw SIM images per second and thus 60 high-resolution reconstructed SIM images per second exceeds that of most commercial systems and is on par with recently published high-speed SIM microscopes [3–8].

Using reference samples and an FRC analysis to assess the spatial resolution that can be achieved with this system, we were able to demonstrate high quality SIM imaging with improved spatial resolution. Images acquired of the actin cytoskeleton and the plasma membrane of fixed U2OS cells additionally support this in a biological context.

In the future, we plan to extend the dual-color DMD-SIM microscope to three colors. Ideally, a laser with a wavelength of $\lambda_3 = 550.7\ nm$ would be suitable for this, hitting the DMD at an angle of $\alpha_3 = -4.3°$. While this precise wavelength is not available, lasers with a wavelength of 550 nm are available [31] and are nevertheless very suitable as a third wavelength. This could be implemented by using the envelope of the γ^- micromirrors, while the $\lambda_1 = 473\ nm$ and $\lambda_2 = 631\ nm$ lasers use the envelope of the γ^+ micromirrors. Thus, the deviation in the wavelength is negligible, since the −4th native diffraction order of λ_3 can be superimposed with the 4th diffraction order of λ_1 and the 3rd diffraction order of λ_2 by small adjustments of the angle of incidence. The resulting asymmetry in the intensity of the Fourier plane of λ_3 is negligibly small.

This approach would thus combine the advantages of Brown et. al. [12], featuring three colors that match well with typical biological imaging applications, while not relying on any moving parts to dynamically adjust the alignment. Such a system should be opto-mechanically simple and stable, cost-effective and compact to build, and provide high-speed three-color SIM imaging.

Funding. Universitätsbibliothek Bielefeld (Publication Fund); Horizon 2020 Framework Programme (752080); Deutsche Forschungsgemeinschaft (415832635).

Acknowledgments. We would like to thank Peter Brown and Douglas Shepherd, for fruitful discussions of the blazed grating effect applied to multi-color SIM illumination and the use of digital micromirror devices in the SIM system. We would also like to thank Alice Sandmeyer for discussing the construction of DMD based SIM systems, and Andreas Markwirth as well as Jochen Linnenbrügger for constructing components for the system. We acknowledge support for the publication costs by the Open Access Publication Fund of Bielefeld University.

Authors' Contributions ML developed the DMD simulation software, the dual color DMD-SIM microscope and drafted the manuscript. GW provided technical support, especially with the lasers and the wavelength tuning via temperature. WH prepared the U2OS cells and carried out their measurement with the dual color DMD-SIM Microscope. TH and JSaE supervised the project and helped write the manuscript. MM envisioned the project and wrote the manuscript. All authors read and approved the manuscript.

Disclosures. The authors declare that they have no competing interests.

Data Availability. The source code of the simulations [13] and the SIM grating search algorithm [7] is available under an open-source (GPLv3) license in online repositories [24,32]. The raw data of the images shown can be found on Zenodo.

Supplemental document. See Supplement 1 for supporting content.

References

1. R. Heintzmann and C. G. Cremer, "Laterally modulated excitation microscopy: improvement of resolution by using a diffraction grating," in I. J. Bigio, H. Schneckenburger, J. Slavik, K. Svanberg, and P. M. Viallet, eds. (*Proc. SPIE*, 1999), 3568, pp. 185–196.
2. M. G. L. Gustafsson, "Surpassing the lateral resolution limit by a factor of two using structured illumination microscopy," J. Microsc. **198**(2), 82–87 (2000).
3. P. Kner, B. B. Chhun, E. R. Griffis, L. Winoto, and M. G. L. Gustafsson, "Super-resolution video microscopy of live cells by structured illumination," Nat. Methods **6**(5), 339–342 (2009).
4. L. Shao, P. Kner, E. H. Rego, and M. G. L. Gustafsson, "Super-resolution 3D microscopy of live whole cells using structured illumination," Nat. Methods **8**(12), 1044–1046 (2011).
5. R. Fiolka, L. Shao, E. H. Rego, M. W. Davidson, and M. G. L. Gustafsson, "Time-lapse two-color 3D imaging of live cells with doubled resolution using structured illumination," PNAS **109**(14), 5311–5315 (2012).

Optics EXPRESS

6. H.-W. Lu-Walther, M. Kielhorn, R. Förster, A. Jost, K. Wicker, and R. Heintzmann, "fastSIM: a practical implementation of fast structured illumination microscopy," Methods Appl. Fluoresc. **3**(1), 014001 (2015).
7. A. Markwirth, M. Lachetta, V. Mönkemöller, R. Heintzmann, W. Hübner, T. Huser, and M. Müller, "Video-rate multi-color structured illumination microscopy with simultaneous real-time reconstruction," Nat. Commun. **10**(1), 4315 (2019).
8. A. Sandmeyer, M. Lachetta, H. Sandmeyer, W. Hübner, T. Huser, and M. Müller, "Cost-Effective Live Cell Structured Illumination Microscopy with Video-Rate Imaging," ACS Photonics **8**(6), 1639–1648 (2021).
9. Y. Wu and H. Shroff, "Faster, sharper, and deeper: structured illumination microscopy for biological imaging," Nat Methods **15**(12), 1011–1019 (2018).
10. R. Heintzmann and T. Huser, "Super-Resolution Structured Illumination Microscopy," Chem. Rev. **117**(23), 13890–13908 (2017).
11. L. Schermelleh, A. Ferrand, T. Huser, C. Eggeling, M. Sauer, O. Biehlmaier, and G. P. C. Drummen, "Super-resolution microscopy demystified," Nat Cell Biol **21**(1), 72–84 (2019).
12. P. T. Brown, R. Kruithoff, G. J. Seedorf, and D. P. Shepherd, "Multicolor structured illumination microscopy and quantitative control of polychromatic light with a digital micromirror device," Biomed. Opt. Express **12**(6), 3700–3716 (2021).
13. M. Lachetta, H. Sandmeyer, A. Sandmeyer, J. S. am Esch, T. Huser, and M. Müller, "Simulating digital micromirror devices for patterning coherent excitation light in structured illumination microscopy," Phil. Trans. R. Soc. A. **379**(2199), 20200147 (2021).
14. J. E. Harvey and R. N. Pfisterer, "Understanding diffraction grating behavior: including conical diffraction and Rayleigh anomalies from transmission gratings," Opt. Eng. **58**(08), 1 (2019).
15. Texas Instruments Incorporated, "Using Lasers with DLP® DMD technology," (2008).
16. Texas Instruments Incorporated, "DLP6500 0.65 1080p MVSP S600 DMD," (2016).
17. "High-end Laser Systems for Scientific and Industry," https://www.toptica.com/.
18. "Oxxius - Simply Light," https://www.oxxius.com/.
19. "Leader in Laser Solutions and Photonics Technology | Coherent," https://www.coherent.com/.
20. "Qioptiq Q-Shop | Präzisionsoptik, Optomechanik, Instrumente," https://www.qioptiq-shop.com/.
21. "HÜBNER Photonics," https://hubner-photonics.com/.
22. Ushio Europe B.V., "633 nm Diodelaser HL63163DG Datasheet," (2021).
23. K. O'Holleran and M. Shaw, "Polarization effects on contrast in structured illumination microscopy," Opt. Lett. **37**(22), 4603 (2012).
24. Fair SIM/Fast SIM-Grating Search https://github.com/fairSIM/fastSIM-GratingSearch (fairSIM, 2019).
25. K. O'Holleran and M. Shaw, "Optimized approaches for optical sectioning and resolution enhancement in 2D structured illumination microscopy," Biomed. Opt. Express **5**(8), 2580 (2014).
26. M. Shaw, L. Zajiczek, and K. O'Holleran, "High speed structured illumination microscopy in optically thick samples," Methods **88**, 11–19 (2015).
27. R. V. den Eynde, W. Vandenberg, S. Hugelier, A. Bouwens, J. Hofkens, M. Müller, and P. Dedecker, "Self-contained and modular structured illumination microscope," bioRxiv 2021.02.25.432746 (2021).
28. M. van Heel and M. Schatz, "Fourier shell correlation threshold criteria," J. Struct. Biol. **151**(3), 250–262 (2005).
29. R. P. J. Nieuwenhuizen, K. A. Lidke, M. Bates, D. L. Puig, D. Grünwald, S. Stallinga, and B. Rieger, "Measuring image resolution in optical nanoscopy," Nat. Methods **10**(6), 557–562 (2013).
30. M. Müller, V. Mönkemöller, S. Hennig, W. Hübner, and T. Huser, "Open-source image reconstruction of super-resolution structured illumination microscopy data in ImageJ," Nat. Commun. **7**(1), 10980 (2016).
31. CNI Lasers, "Green laser, Blue laser, Infra Red laser, IR laser, UV DPSS laser.," http://www.cnilaser.com/.
32. *Biophotonics-Bielefeld/Coherent-Dmd-Sim-Simulator* (Biophotonics Bielefeld, 2021). https://github.com/biophotonics-bielefeld/coherent-dmd-sim-simulator